ISSN 1066-3622, Radiochemistry, 2019, Vol. 61, No. 4, pp. 434–442. © Pleiades Publishing, Inc., 2019.

Synthesis, Characterization, and X-ray Structure of Tetraaminoguanidinium Diuranyl Tetraoxalate Monohydrate $(HAgun)_4[(UO_2)_2(C_2O_4)_4]\cdot H_2O$

T. M. Ahamed Hussain[a] and B. N. Sivasankar[a]*

Department of Chemistry, Government Arts College, Udhagamandalam, Nilgiris-643002, India
**e-mail: sivabickol@yahoo.com*

Received May 8, 2018; revised May 18, 2019; accepted May 23, 2019

Abstract—A new uranyl oxalate complex containing aminoguanidinium cation was isolated from an aqueous solution containing uranyl nitrate hexahydrate, oxalic acid dihydrate, and aminoguanidinium bicarbonate in appropriate ratio. The compound was characterized by analytical, spectral (UV-Vis and IR), and thermal (TG–DTA) techniques. The X-ray crystallographic study shows that the complex has a polymeric structure with two types of coordination around the alternative uranyl ions. The oxalate ions exhibit tetradentate bridging and tridentate bridging modes. The aminoguanidinium cation is in the outer sphere, acting as charge-neutralizing species. An intense photoluminescence peak is observed at 519 nm. The thermal decomposition of the complex yields U_3O_8. SEM photographs of U_3O_8 show the presence of irregularly shaped agglomerated particles of submicron size.

Keywords: aminoguanidinium cation, uranyl ion, oxalates, X-ray crystal structure, TG–DTA, photoluminescence, EDX, SEM

DOI: 10.1134/S1066362219040064

INTRODUCTION

Actinide chemistry is being extensively studied [1–3]. Among the actinides, the most important and well studied element is uranium. Uranium can exist in oxidation states ranging from +2 to +6 [4], and in each oxidation state uranium has quite different chemical properties. Complexes of uranyl ion with simple organic chelating ligands like oxalate ion are particularly attractive because of their versatility, utility, and structure. Oxalic acid is often used as a precipitating agent for waste decontamination in nuclear fuel technology and as a complexing agent to adjust the extraction characteristics of actinides and lanthanides or redox behavior of actinides [5]. The chemical properties of actinide and lanthanide oxalates have been extensively studied, and the crystal structures of many complexes have been determined. Oxalate ion can be coordinated in diverse modes: monodentate to tetradentate, chelating and bridging. The geometry and coordination number of the metal ion actually depend on the coordination mode of the oxalate ion in the particular complex. The auxiliary ligand or charge-neutralizing species and water molecules also affect the geometry and properties of the complexes.

Hydrazine and sodium uranyl oxalates have interesting structures, and uranium in these complexes exhibits different coordination numbers. Several uranium complexes with coordination number 7 such as $(N_2H_5)_2[UO_2(C_2O_4)_2(H_2O)]$ [6], $(NH_4)_2[UO_2(C_2O_4)_2\cdot(H_2O)]\cdot 2H_2O$ [7], and $Na_2[UO_2(C_2O_4)(H_2O)_2]\cdot 4H_2O$ and the complex with coordination number 8, $(NH_4)_4\cdot[UO_2(C_2O_4)_3]$ [8], have been reported, and their structures were studied in detail. Similar complexes with monocarboxylic acids such as $N_2H_5[UO_2(CH_3COO)_3]$ and $N_2H_5[UO_2(CH_3CH_2COO)_3]$ have been isolated as single crystals, and their spectral, thermal, and structural properties have been extensively studied [9]. Though several oxalate complexes of uranyl ion have been isolated, in the uranyl oxalate system there is still a space for research. This is due to the fact that the counterion plays an equally important role in designing the geometry of these complexes.

We have reported several hydrazinium metal carboxylates [10–14]. Recently, we have reported similar aminoguanidinium complexes with transition metal carboxylates. The growing interest in these hydrazinium and aminoguanidinium complexes is due to the coordination ability of the cations and the thermal re-

activity of their complexes. The N–N bond present in these cations is endothermic in nature and undergoes exothermic degradation during the pyrolysis of their complexes. Furthermore, aminoguanidinium complexes are safer to handle than hydrazine complexes because of violent decomposition of the latter compounds. The instability of the hydrazine complexes complicates isolation of the oxide material and affects the particle size and quality of the oxide formed by thermal decomposition. Here we report the synthesis, spectral, thermal, photoluminescent properties, and crystal structure of a new tetraaminoguanidinium diuranyl tetraoxalate, $(HAgun)_4[(UO_2)_2(C_2O_4)_4]\cdot H_2O$. We also report the properties of the oxide U_3O_8 obtained by thermal decomposition of the complex.

EXPERIMENTAL

Materials and methods. All the chemicals and solvents were purchased from S.D. Fine Chemicals, Mumbai, India. The hydrazine content was determined by volumetric analysis using a 0.025 M KIO_3 solution under Andrew's conditions. The U(VI) content was determined gravimetrically using 2-quinolinol [16, 17]. The CHN analyses were carried out with a Perkin–Elmer 2400 CHN elemental analyzer. The IR spectrum of the complex (KBr disc) was recorded in the range 400–4000 cm^{-1} on a Bruker Alpha spectrophotometer. The simultaneous TG–DTA of the sample in air was performed with an SWI TG/DTA 6200 thermal analyzer; a ~5-mg portion of the sample was heated at a rate of 10°C min^{-1} in a platinum cup. The set of single crystal reflection intensities was collected on an Enraf-Nonius CAD-4 diffractometer using graphite-monochromated MoK_α radiation (λ = 0.71073 Å). The structure of the complex was solved by the direct method using SIR 92 program, completed using Fourier techniques, and refined by the full-matrix least-squares techniques. The refinement was carried out using SHELXL-2014 program [18, 19]. Crystallographic data of the complex have been deposited at the Cambridge Crystallographic Data Centre (CCDC no. 1913491). The fluorescence spectrum was recorded using a Cary Eclipse Spectrometer. The X-ray powder diffraction pattern of the metal oxide was recorded with a Philips PW 1050/70 device using CuK_α radiation (λ = 1.5406 Å) with an iron filter. The measurements were taken in the range of 2θ from 20° to 80°. The morphology and microstructure of the metal oxide were examined with a Quanta FEG-250 field-emission scanning electron microscope (SEM) equipped with Bruker EDX.

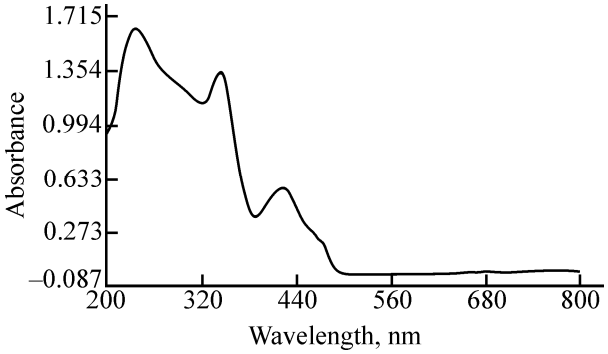

Fig. 1. Electronic absorption spectrum of $(HAgun)_4[(UO_2)_2\cdot(C_2O_4)_4]\cdot H_2O$.

Preparation of $(HAgun)_4[(UO_2)_2(C_2O_4)_4]\cdot H_2O$. An aqueous solution (50 mL) containg 5.02 g (0.01 mol) of $UO_2(NO_3)_2\cdot 6H_2O$ was mixed with an aqueous solution containing a mixture of oxalic acid dihydrate (1.26 g, 0.01 mol) and aminoguanidinium bicarbonate (4.08 g, 0.03 mol). The resulting solution after filtration was allowed to crystallize at room temperature. Pure and homogeneous yellow crystals of the complex were obtained after 15 days. These crystals were filtered off, washed quickly with ice-cold water, and dried in air. Yield 62%. Elemental analysis, found, %: C 12.44, H 1.88, N 15.10, U 40.65; calculated, %: C 12.00, H 1.67, N 14.09, U 39.93. N_2H_4, found (calculated), %: 5.50 (5.36).

RESULTS AND DISCUSSION

Electronic spectrum. The electronic spectrum of the complex has broad bands in the visible region from 21100 to 23500 cm^{-1} (Fig. 1), assigned to the $^1\Sigma \rightarrow {}^3\Pi_g^+$ transition of the uranyl ion [15].

IR spectrum. The IR spectrum of the complex has two bands in the region of 930 and 840 cm^{-1}, assigned to asymmetric and symmetric stretching vibrations, respectively, of the uranyl cation. The N–N stretching mode of the hydrazine moiety of the aminoguanidinium cation is manifested at 1095 cm^{-1} [20, 21]. A broad split band appears around 3300–3400 cm^{-1}; it is assigned to different types of N–H stretching vibrations of the aminoguanidinium ion [22]. Strong to medium-intensity bands originating from the asymmetric stretching vibrations of the carboxylate group are observed in the range 1685–1655 cm^{-1}, whereas the symmetric stretching vibrations are observed between 1450

Table 1. Thermal data for $(HAgun)_4[(UO_2)_2(C_2O_4)_4]\cdot H_2O$

DTA peak temperature, °C	TG temperature range,[a] °C	TG weight loss, %		Decomposition product
		found	calculated	
90(+)	40–120	2.00	1.48	H_2O
180(+)	160–240	24.50	25.15	$[UO_2(C_2O_4)](Agun)_2$
360(–)	240–325	39.50	38.85	$[UO_2(C_2O_4)]$
480(–)	325–560	48.00	46.95	U_3O_8

[a] (+) Endothermic and (–) exothermic.

and 1430 cm^{-1}. The IR spectrum of the complex is shown in Fig. 2.

Thermal degradation studies. Simultaneous TG–DTA of the complex (Fig. 3) shows that its decomposition is multistep. Initially the removal of lattice water with 2% weight loss takes place. The corresponding weak endothermic peak is observed in the DTA curve at 90°C. In the second step, four aminoguanidine molecules are eliminated to yield uranyl oxalate as an intermediate. However, the DTA shows two endothermic peaks suggesting the elimination of two aminoguanidine molecules below 200°C and of the other two molecules between 200–240°C. The uranyl oxalate

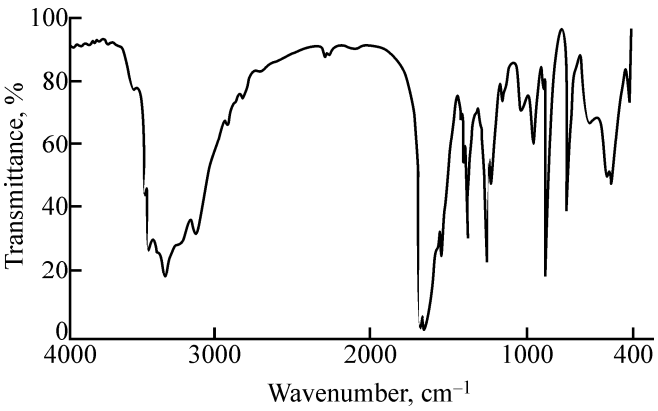

Fig. 2. IR spectrum of $(HAgun)_4[(UO_2)_2(C_2O_4)_4]\cdot H_2O$.

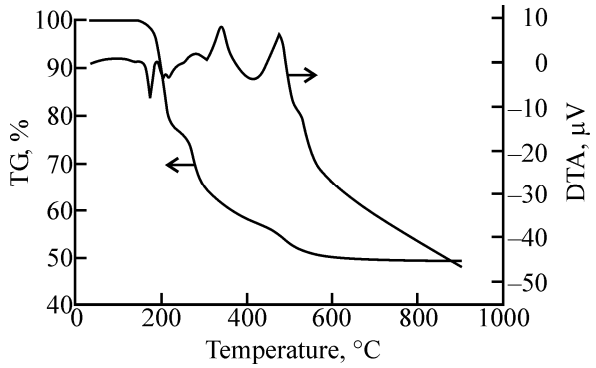

Fig. 3. Simultaneous TG–DTA of $(HAgun)_4[(UO_2)_2(C_2O_4)_4]\cdot H_2O$.

Table 2 Crystal data and structure refinement for $(HAgun)_4\cdot[(UO_2)_2(C_2O_4)_4]\cdot H_2O$

Parameter	Value
Empirical formula	$C_{12}H_{30}N_{16}O_{21}U_2$
Formula weight	1210.58
Temperature	295(2) K
Wavelength	0.71073 Å
Crystal system	Triclinic
Space group	$P\bar{1}$
a, Å	10.6085(6)
b, Å	11.1379(6)
c, Å	14.8039(8)
α, deg	81.355(2)
β, deg	70.896(2)
γ, deg	77.042(2)
Unit cell volume, $Å^3$	1605.12(15)
Z	2
Density (calculated)	2.505 Mg m^{-3}
Absorption coefficient	10.186 mm^{-1}
F(000)	1132
Crystal size, mm	0.150 × 0.100 × 0.100
θ range for data collection, deg	2.873–24.999
Index ranges	$-12 \le h \le 12$, $-13 \le k \le 13$, $-17 \le l \le 17$
Reflections collected	48 941
Independent reflections	5644 [*R*(int) = 0.0365]
Completeness to θ = 24.999°	99.7%
Absorption correction	Semiempirical from equivalents
Maximal and minimal transmission	0.7467 and 0.4247
Refinement method	Full-matrix least-squares on F^2
Data/restraints/parameters	5644/44/550
Goodness-of-fit on F^2	1.283
Final *R* indices [$I > 2\sigma(I)$]	*R*1 = 0.0300, *wR*2 = 0.0664
R indices (all data)	*R*1 = 0.0385, *wR*2 = 0.0729
Extinction coefficient	Not applied
Largest diff. peak and hole	2.541 and –1.842 e $Å^{-3}$

Table 3 Selected bond lengths (*d*) and angles (ω) for $(HAgun)_4[(UO_2)_2(C_2O_4)_4]\cdot H_2O$

Bond	*d*, Å	Angle	ω, deg	Angle	ω, deg
U(1)–O(10)	1.764(6)	O(10)–U(1)–O(9)	178.7(3)	O(20)–U(2)–O(19)	179.2(3)
U(1)–O(9)	1.766(6)	O(10)–U(1)–O(3)	85.5(3)	O(20)–U(2)–O(15)	90.3(2)
U(1)–O(3)	2.417(5)	O(9)–U(1)–O(3)	95.7(3)	O(19)–U(2)–O(15)	89.8(2)
U(1)–O(1)	2.435(6)	O(10)–U(1)–O(1)	96.7(2)	O(20)–U(2)–O(11)	90.5(2)
U(1)–O(5)	2.481(5)	O(9)–U(1)–O(1)	83.9(2)	O(19)–U(2)–O(11)	90.3(2)
U(1)–O(17)	2.502(5)	O(3)–U(1)–O(1)	64.33(18)	O(15)–U(2)–O(11)	77.90(18)
U(1)–O(18)	2.531(6)	O(10)–U(1)–O(5)	83.6(2)	O(20)–U(2)–O(13)	94.0(2)
U(1)–O(8)	2.555(5)	O(9)–U(1)–O(5)	95.7(2)	O(19)–U(2)–O(13)	86.3(2)
U(2)–O(20)	1.762(5)	O(3)–U(1)–O(5)	123.10(18)	O(15)–U(2)–O(13)	144.17(18)
U(2)–O(19)	1.776(5)	O(1)–U(1)–O(5)	61.85(18)	O(11)–U(2)–O(13)	66.54(17)
U(2)–O(15)	2.351(5)	O(10)–U(1)–O(17)	87.7(2)	O(20)–U(2)–O(6)	94.0(2)
U(2)–O(11)	2.359(5)	O(9)–U(1)–O(17)	91.9(2)	O(19)–U(2)–O(6)	85.3(2)
U(2)–O(13)	2.390(5)	O(3)–U(1)–O(17)	112.54(18)	O(15)–U(2)–O(6)	74.67(18)
U(2)–O(6)	2.425(5)	O(1)–U(1)–O(17)	174.3(2)	O(11)–U(2)–O(6)	152.22(17)
U(2)–O(7)	2.438(5)	O(5)–U(1)–O(17)	122.53(17)	O(13)–U(2)–O(6)	140.15(16)
N(3)–N(4)	1.399(10)	O(10)–U(1)–O(18)	95.4(3)	O(20)–U(2)–O(7)	84.2(2)
N(7)–N(8)	1.401(10)	O(9)–U(1)–O(18)	85.2(3)	O(19)–U(2)–O(7)	95.2(2)
N(11)–N(12)	1.386(11)	O(3)–U(1)–O(18)	63.27(18)	O(15)–U(2)–O(7)	139.88(18)
N(15)–N(16)	1.393(10)	O(1)–U(1)–O(18)	124.81(19)	O(11)–U(2)–O(7)	41.61(17)
O(21)–H(21A)	0.85(2)	O(5)–U(1)–O(18)	173.33(18)	O(13)–U(2)–O(7)	75.94(16)
O(21)–H(21B)	0.85(2)	O(17)–U(1)–O(18)	50.80(18)	O(6)–U(2)–O(7)	66.17(16)
		O(10)–U(1)–O(8)	96.5(2)	O(12)–C(2)–C(1)	116.8(4)
		O(9)–U(1)–O(8)	82.2(2)	N(9)–C(11)–N(10)	120.5(8)
		O(3)–U(1)–O(8)	173.47(17)	N(15)–C(12)–N(13)	120.1(8)
		O(1)–U(1)–O(8)	121.40(17)	N(14)–C(12)–N(13)	120.6(8)
		O(5)–U(1)–O(8)	63.38(16)	N(1)–C(9)–N(2)	121.4(8)

formed undergoes exothermic decomposition at a higher temperature to yield U_3O_8 as the final residue. The observed TG weight losses agree very well with the calculated values. The proposed decomposition scheme is shown below. The thermal data for the complex are given in Table 1.

$$(HAgun)_4[(UO_2)_2(C_2O_4)_4]\cdot H_2O$$
$$\downarrow 40\text{–}120^\circ C$$
$$(HAgun)_4[(UO_2)_2(C_2O_4)_4]$$
$$\downarrow 160\text{–}200^\circ C$$
$$2UO_2(C_2O_4)(Agun)_2$$
$$\downarrow 200\text{–}240^\circ C$$
$$2UO_2(C_2O_4)$$
$$\downarrow 240\text{–}560^\circ C$$
$$2/3\ U_3O_8$$

Crystal structure of $(HAgun)_4[(UO_2)_2(C_2O_4)_4]\cdot H_2O$. The compound $(HAgun)_4[(UO_2)_2(C_2O_4)_4]\cdot H_2O$ is a 1 : 4 tetraanionic complex. This complex crystallizes in a triclinic system with $P\bar{1}$ space group. The crystal and structure refinement data are given in Table 2, and

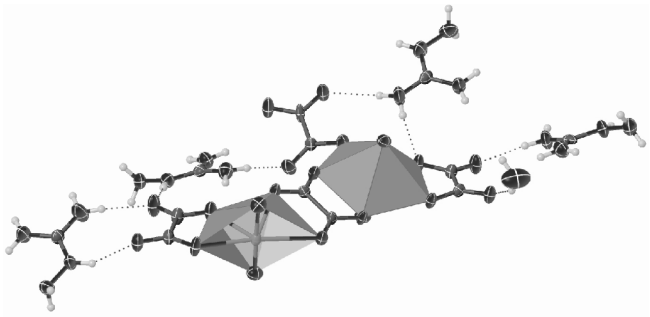

Fig. 4. Polyhedron crystal structure of $(HAgun)_4[(UO_2)_2\cdot(C_2O_4)_4]\cdot H_2O$.

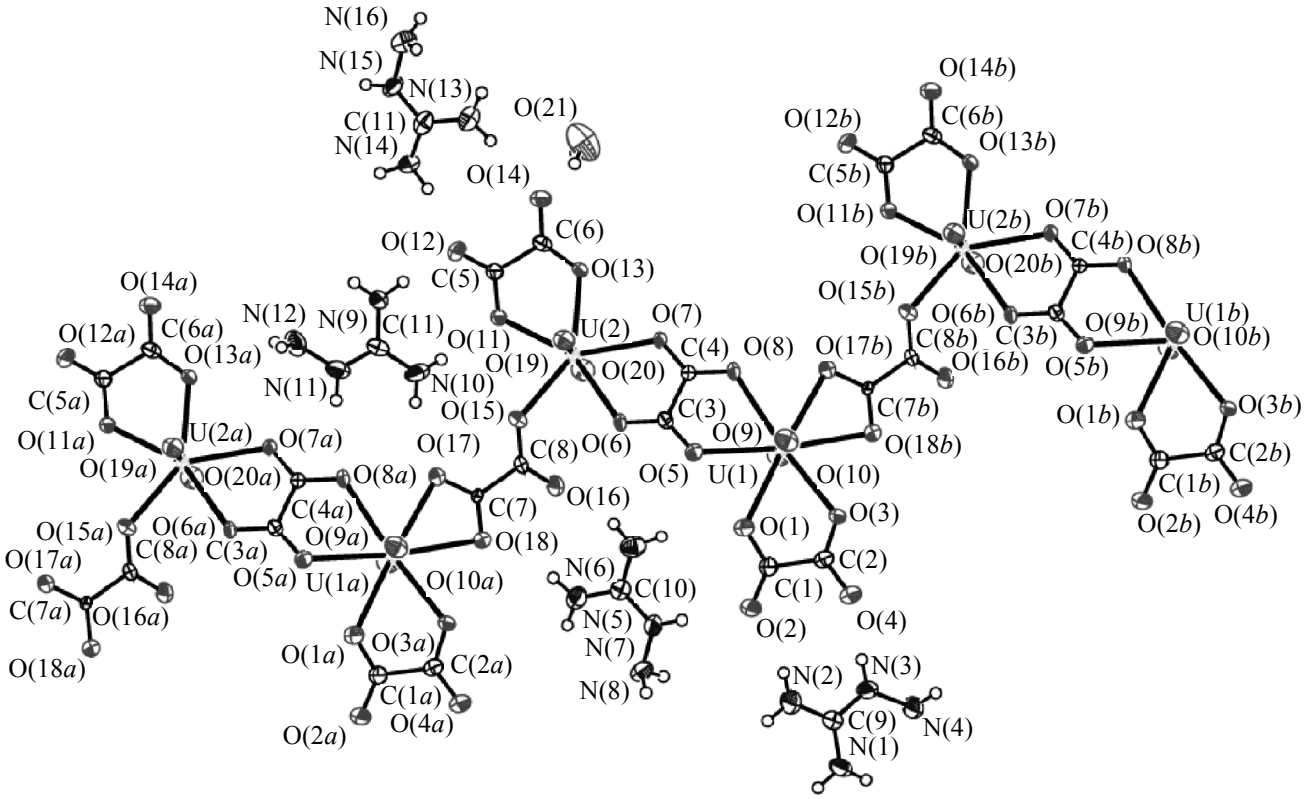

Fig. 5. ORTEP diagram of $(HAgun)_4[(UO_2)_2(C_2O_4)_4]\cdot H_2O$ (50% probability level).

the selected bond length and bond angles are listed in Table 3. The crystal structure (Fig. 4) of the complex is a two-dimensional polymeric structure with oxalate bridges. The adjacent uranyl ions show two types of coordination behavior, with pentagonal bipyramidal and hexagonal bipyramidal geometries around alternative uranium atoms. The eight-coordinate uranium atom is surrounded by two uranyl oxygen atom with shorter bonds (1.764 Å and 1.776 Å) and six bidentate chelating carboxylate oxygen atoms from three different oxalate ions with longer U–O bonds (2.4–2.6 Å). Among the three oxalate ions, two are tetradentate chelating and one is tridentate chelating. Thus, oxalate ions also show two types of coordination behavior, with both acting as bridging ligands. The aminoguanidinium cations are present as discrete ions and occupy the outer coordination sphere as charge-neutralizing species. The aminoguanidinium cation is not coordinated to uranium, apparently because of the lack of space in the coordination sphere, despite the presence of four coordination sites (four nitrogen atoms). However, the cations are involved in strong hydrogen bonding with oxalate oxygen atoms along with water molecule, which stabilizes the whole system.

The distance between two uranium atoms, U(1) and U(2), is 6.376 Å, and the U–O (oxalate) distance varies from 2.428(5) to 2.557(5) Å with an average value of 2.492 Å (Fig. 5). The uranyl group has a typical linear O–U–O geometry with an average U–O distance of 1.765 Å and O–U–O angle of 179.0(3)°. Two oxygen atoms of the O=U=O group occupy the axial positions. The six oxygen atoms around U(1) and five around U(2) occupy the corners of the planar hexagon and planar pentagon, respectively. These results are in good agreement with the earlier reports [23, 24]. The packing diagram of the complex is shown in Fig. 6. The hydrogen bonding data are given in Table 4. The unit cell consists of two hydrogen-bonded molecules. The hydrogen bonds are formed between the oxygen atom of the oxalate ion and hydrogen atoms of the aminoguanidinium ions (O···H–N) and also with the water molecule. Hydrogen bonding is also observed between the aminoguanidine cations (N–H···N). The N–N bond distances in the crystallographically independent cations vary from 1.404(10) to 1.377(10) Å

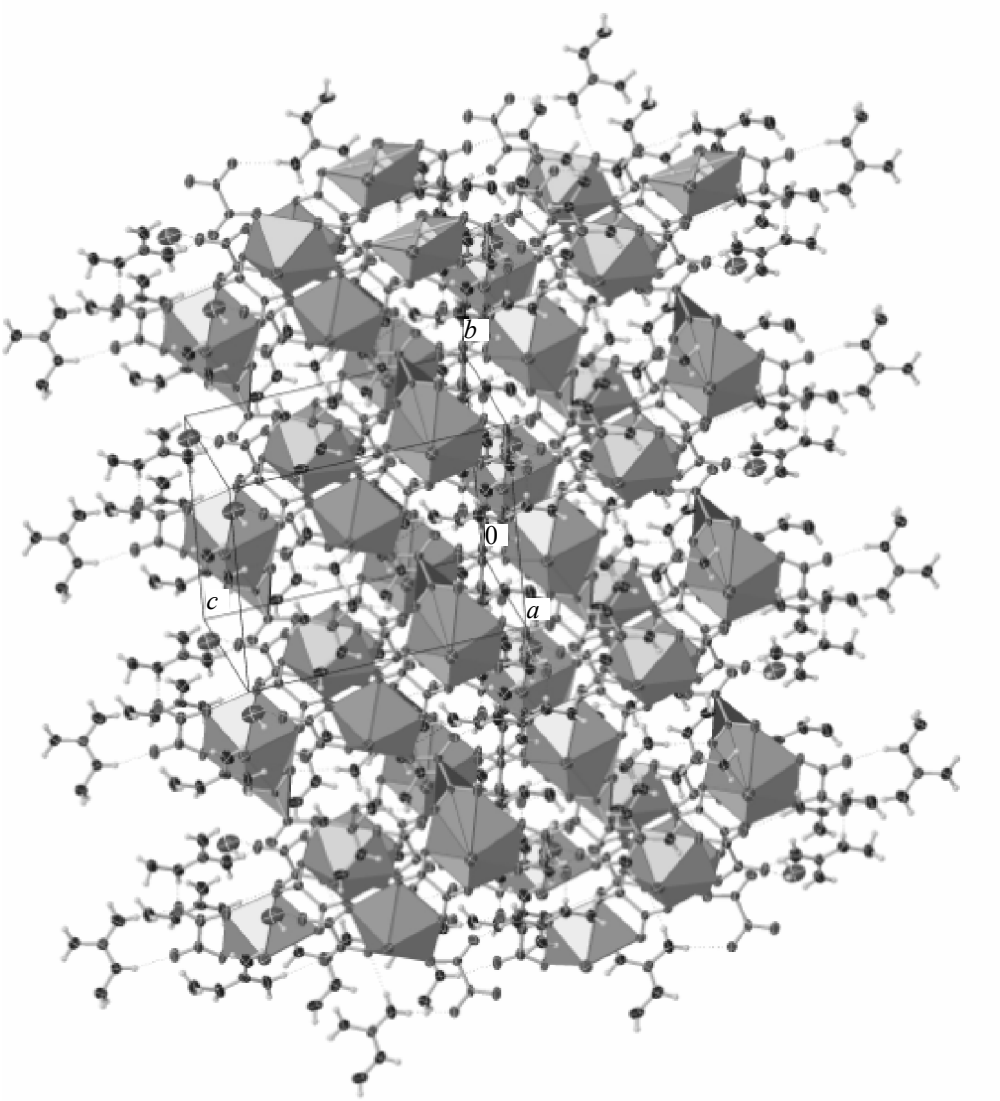

Fig. 6. Polyhedron packing diagram of $(HAgun)_4[(UO_2)_2(C_2O_4)_4]\cdot H_2O$.

with an average value of 1.394 Å. These values are comparable with those in the previously reported aminoguanidinium complexes [25].

Photoluminescence studies. The photoluminescence spectra of the uranyl complexes are located in the visible region (480–600 nm) [26]. Fluorescence spectra of uranyl complexes typically have characteristic six peaks related to the $S_{11} \rightarrow S_{00}$ and $S_{10} \rightarrow S_{0n}$ electronic transitions, where n = 0–4; for $UO_2\cdot(CH_3COO)_2\cdot 2H_2O$, the most intense peak ($S_{10} \rightarrow S_{00}$) is positioned at 508 nm [27]. The luminescence of tetraaminoguanidinium diuranyl tetraoxalate was studied at the excitation wavelength of 370 nm, and seven peaks (398, 420, 438, 497, 519, 542, 568 nm) were observed (Fig. 7). The peak of 398 nm was attributed to the ligand-to-metal charge transfer (LMCT). The most intense peak located at 519 nm exhibited red shift compared to the benchmark compound $UO_2(CH_3COO)_2\cdot 2H_2O$ [28].

Powder X-ray diffraction. On complete pyrolysis, the precursor complex yielded uranium oxide U_3O_8 as the final residue. The formation of U_3O_8 is confirmed by powder X-ray diffraction (PXRD) technique. The powder X-ray diffraction pattern of the oxide is shown in Fig. 8. The lines observed at d values of 4.21, 3.46, 3.38, 2.66, and 2.08 Å correspond closely to {001}, {130}, {131}, {200} and {002} reflections of α-U_3O_8 (JCPDS card no. 24-1172). The U_3O_8 crystallite size

Table 4. Hydrogen bonding interactions for $(HAgun)_4[(UO_2)_2(C_2O_4)_4]\cdot H_2O$

D–H···A	*d*(D–H), Å	*d*(H···A), Å	*d*(D···A), Å	DHA angle, deg	Symmetry code for A
N(1)–H(1A)···N(4)	0.84(2)	2.40(6)	3.124(11)	146(8)	–*x* + 2, –*y* + 2, –*z* – 1
N(2)–H(2A)···O(13)	0.84(2)	2.46(4)	3.248(10)	157(10)	*x* + 1, *y*, *z* – 1
N(2)–H(2A)···O(14)	0.84(2)	2.34(6)	3.049(10)	142(8)	*x* + 1, *y*, *z* – 1
N(2)–H(2B)···O(2)	0.84(2)	1.99(5)	2.793(10)	158(11)	–
N(3)–H(3A)···O(4)	0.85(2)	2.13(5)	2.891(9)	149(9)	–
N(4)–H(4A)···O(8)	0.86(2)	2.37(4)	3.177(10)	157(7)	–*x* + 1, –*y* + 2, –*z*
N(4)–H(4B)···O(12)	0.85(2)	2.26(2)	3.102(10)	171(8)	*x* + 1, *y* + 1, *z* – 1
N(5)–H(5A)···O(16)	0.85(2)	2.56(6)	3.160(10)	129(7)	–
N(5)–H(5A)···O(18)	0.85(2)	2.40(5)	3.187(9)	156(9)	–
N(5)–H(5B)···O(9)	0.85(2)	2.49(4)	3.301(10)	159(7)	–*x* + 1, –*y* + 1, –*z*
N(6)–H(6A)···O(16)	0.84(2)	2.14(4)	2.925(10)	155(9)	–
N(6)–H(6B)···O(1)	0.84(2)	2.33(3)	3.151(10)	166(7)	–
N(6)–H(6B)···O(21)	0.84(2)	2.84(10)	3.071(11)	98(7)	–*x* + 1, –*y* + 1, –*z* + 1
N(7)–H(7A)···O(2)	0.85(2)	2.03(2)	2.872(9)	179(9)	–
N(8)–H(8B)···O(20)	0.86(2)	2.87(7)	3.331(9)	115(6)	–*x* + 1, –*y* + 1, –*z*
N(9)–H(9A)···O(10)	0.84(2)	2.48(7)	3.126(10)	134(9)	–*x* + 1, –*y* + 1, –*z* + 1
N(9)–H(9A)···O(12)	0.84(2)	2.44(6)	3.145(10)	141(9)	–
N(9)–H(9B)···N(16)	0.85(2)	2.14(3)	2.978(11)	167(7)	–*x*, –*y*, –*z* + 2
N(10)–H(10A)···O(17)	0.84(2)	2.13(6)	2.909(9)	154(11)	–
N(10)–H(10B)···O(11)	0.83(2)	2.14(2)	2.970(10)	174(9)	–
N(10)–H(10B)···O(15)	0.83(2)	2.68(9)	3.081(10)	111(8)	–
N(11)–H(11A)···O(8)	0.85(2)	2.37(5)	3.147(9)	152(9)	*x*, *y* – 1, *z*
N(11)–H(11A)···O(19)	0.85(2)	2.57(8)	3.158(9)	127(9)	–*x* + 1, –*y*, –*z* + 1
N(12)–H(12B)···O(6)	0.85(2)	2.25(3)	3.090(10)	170(9)	–*x* + 1, –*y*, –*z* + 1
N(13)–H(13A)···O(21)	0.85(2)	2.21(4)	3.023(12)	160(10)	–*x*, –*y* + 1, –*z* + 2
N(13)–H(13B)···O(14)	0.85(2)	2.38(4)	3.180(10)	157(9)	–
N(14)–H(14A)···O(4)	0.85(2)	2.07(4)	2.889(10)	161(9)	*x* – 1, *y* – 1, *z* + 1
N(14)–H(14B)···O(12)	0.85(2)	2.01(4)	2.825(9)	160(9)	–
N(15)–H(15A)···O(3)	0.85(2)	2.24(3)	3.073(9)	165(9)	*x* – 1, *y* – 1, *z* + 1
N(16)–H(16B)···O(21)	0.84(2)	2.65(5)	3.123(12)	117(4)	–*x*, –*y* + 1, –*z* + 2
O(21)–H(21A)···O(14)	0.85(2)	1.99(6)	2.772(9)	151(10)	–
O(21)–H(21B)···O(5)	0.85(2)	2.47(3)	3.322(11)	175(13)	–*x* + 1, –*y* + 1, –*z* + 1

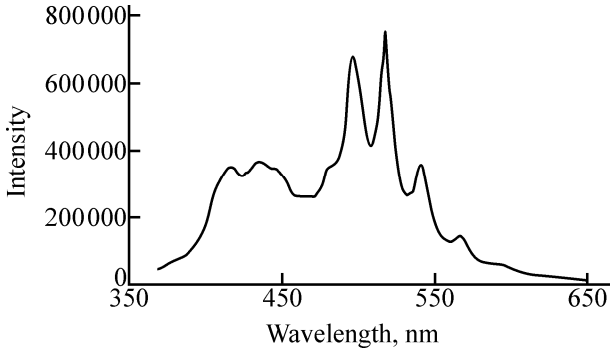

Fig. 7. Photoluminescence spectrum of $(HAgun)_4[(UO_2)_2\cdot(C_2O_4)_4]\cdot H_2O$.

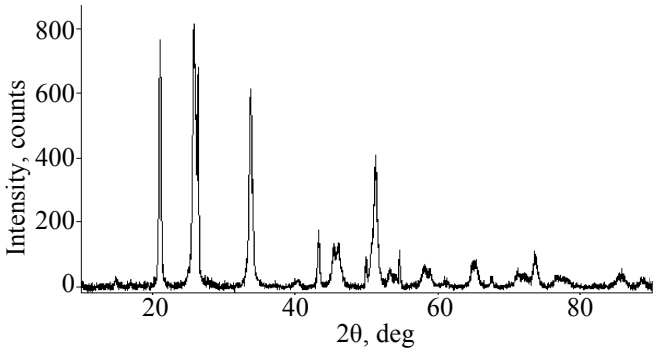

Fig. 8. Powder X-ray diffraction pattern of U_3O_8.

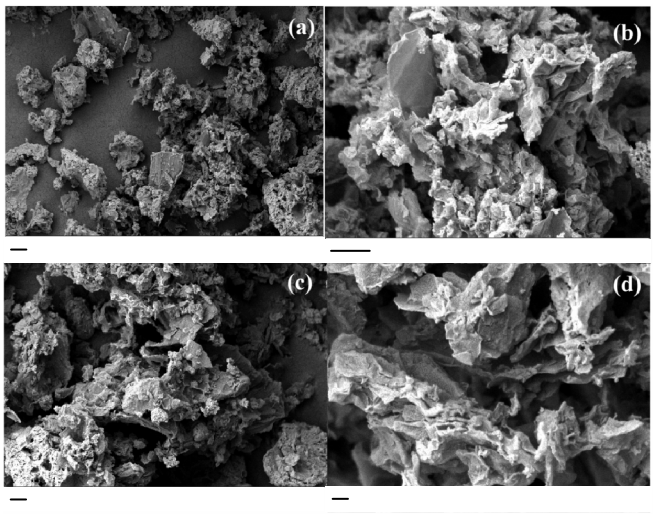

Fig. 9. SEM images of U_3O_8. Scale: (a) 2 μm, (b, c) 1 μm, and (d) 200 nm.

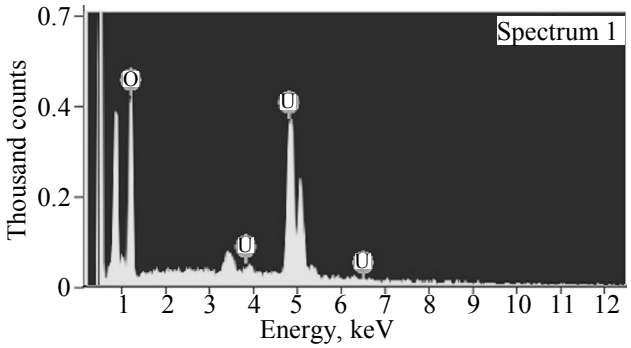

Fig. 10. Energy-dispersive X-ray (EDX) elemental mapping of U_3O_8.

was calculated by the Debye–Scherrer formula. The crystallite size obtained from the peak of maximum intensity, {130}, is 16.01 nm.

Scanning electron microscopy (SEM) and energy-dispersive X-ray (EDX) analysis. The structural morphology of the oxide obtained from the complex precursor was examined by SEM. Numerous voids and cracks can be seen, suggesting abundant gas evolution during the decomposition. The SEM photographs of the oxide, taken at different magnifications, are shown in Fig. 9. These photographs also reveal the presence of irregularly shaped agglomerated particles of submicron size. The EDX data clearly show the presence of uranium and oxygen in the residue (Fig. 10).

ACKNOWLEDGMENTS

One of the authors, (T.M. Ahamed Hussain) is grateful to the University Grants Commission, New Delhi for RGNFD fellowship (Ref. no. F/2016-17/RGNFD-2016-17-TAM-2463).

CONFLICT OF INTEREST

The authors declare that they have no conflict of interest.

REFERENCES

1. Katz, J.J., Morss, L.R., and Seaborg, G.T., *The Chemistry of the Actinide and Transactinide Elements*, Dordrecht: Springer, 2011, vols. 1–6.
2. Moore, K.T. and Vanderlaan, G., *Rev. Mod. Phys*., 2009, vol. 81, pp. 235–298.
3. Ephritikhine, M., *Dalton Trans*., 2006, pp. 2501–2516.
4. MacDonald, M.R., Fieser, M.E., Bates, J.E., et al., *J. Am. Chem. Soc*., 2013, vol. 135, pp. 13 310–13 313.
5. Ferri, D., Iuliano, M., Manfredi, C., et al., *J. Chem. Soc., Dalton Trans*., 2000, pp. 3460–3466.
6. Poojary, M.D. and Patil, K.C., *Proc. Indian Acad. Sci*., 1987, vol. 99, pp. 311–315.
7. Chapelet-Arab, B., Nowogrocki, G., Abraham, F., and Grandjean, S., *Radiochim. Acta*, 2005, vol. 93, pp. 279–286.
8. Baeva, E.E., Mikhailov, Yu.N., Gorbunova, Yu.E., et al., *Russ. J. Inorg. Chem*., 2002, vol. 47, no. 9, pp. 1348–1356.
9. Subramani, B., Sivasankar, B.N., and Wilfred Sugumar, R., *Int. J. Chem*., 2014, vol. 3, no. 1, pp. 27–34.
10. Ragul, R. and Sivasankar, B.N., *Sci. Rev. Chem. Commun*., 2013, vol. 3, no. 1, pp. 81–93.
11. Kuppusamy, K., Sivasankar, B.N., and Govindarajan, S., *Thermochim. Acta*, 1995, vol. 259, pp. 251–262.
12. Sivasankar, B.N., Sharmila, J.R., and Ragunath, L., *Synth. React. Inorg. Met.-Org. Chem*., 2004, vol. 34, pp. 1787–1800.
13. Vikram, L. and Sivasankar, B.N., *J. Therm. Anal. Calorim*., 2008, vol. 91, pp. 963–970.
14. Vikram, L. and Sivasankar, B.N., *Indian J. Chem*., 2007, vol. 46, pp. 568–575.
15. Erdey, L. and Buzaz, I., *Gravimetric Analysis*, London: Pergamon, 1965, part II.
16. Vogels, A.I., *A Textbook of Quantitative Inorganic Analysis*, London: Longmans, 1962, 3rd ed.
17. Johnson, C.K., *ORTEP ORNL-3794*, Tennessee: Oak Ridge National Laboratory, 1976.
18. Sheldrick, G.M., *SHELXL-2014 Programs for Crystal Structure Determination*, England: Univ. of Cambridge, 2015.

19. McGlynn, S.P. and Smith, J.K., *J. Mol. Spectrosc*., 1961, vol. 6, pp. 164–187.
20. Saveleva, Z.A., Romanenko, G.V., Sheludyakova, L.A., and Larionov, S.V., *Polyhedron*, 2000, vol. 17, pp. 1737–1740.
21. Ugono, O., Rath, N.P., and Beatty, A.M., *Cryst. Growth Des*., 2009, vol. 9, pp. 4595–4598.
22. Packiaraj, S., Pushpaveni, A., Govindarajan, S., and Rawson, J.M., *CrystEngComm*, 2016, vol. 18, pp. 7978–7993.
23. Klampfer, P., Benkic, P., Ponikvar, M., et al., *Monatsh. Chem*., 2003, vol. 134, pp. 1–9.
24. Selvakumar, R., Geib, S.J., Premkumar, T., and Govindarajan, S., *Polyhedron*, 2015, vol. 87, pp. 321–328.
25. Selvakumar, R., Geib, S.J., Premkumar, T., and Govindarajan, S., *J. Therm. Anal, Calorim*., 2016, vol. 124, pp. 375–385.
26. Bell, J.T. and Biggers, R.E., *J. Mol. Spectrosc*., 1968, vol. 25, pp. 312–329.
27. Lauren, A.B. and Christopher, L.C., *Cryst. Growth Des*., 2006, vol. 6, pp. 2248–2259.
28. Zhai, X.S., Zhu, W.G., Xu, W., et al., *CrystEngComm*, 2015, vol. 17, pp. 2376–2388.